HHS Public Access

Author manuscript

Mater Horiz. Author manuscript; available in PMC 2019 September 16.

Published in final edited form as:

Mater Horiz. 2017 November 1; 4(6): 1092–1101. doi:10.1039/C7MH00442G.

$LiGa_5O_8$:Cr-based theranostic nanoparticles for imaging-guided X-ray induced photodynamic therapy of deep-seated tumors

Hongmin Chen[#†,‡,§], **Xilin Sun**[#†], **Geoffrey D. Wang**[‡], **Koichi Nagata**[#], **Zhonglin Hao**[‖], **Andrew Wang**[¶], **Zibo Li**[Δ], **Jin Xie**[‡,*], **Baozhong Shen**[†,*]

[†]Molecular Imaging Research Center (MIRC), TOF-PET/CT/MR center, The Fourth Hospital of Harbin Medical University, Harbin Medical University, Harbin, Heilongjiang 150028, China

[‡]Department of Chemistry, University of Georgia, Athens, Georgia 30602, USA

[§]Center for Molecular Imaging and Translational Medicine, State Key Laboratory of Molecular Vaccinology and Molecular Diagnostics, School of Public Health, Xiamen University, Xiamen 361102, China

[#]College of Veterinary Medicine, University of Georgia, Athens, GA 30602, USA

[‖]Section of Hematology and Oncology, Georgia Cancer Center, Medical College of Georgia, Augusta University, Augusta, Georgia 30912, USA

[¶]Department of Radiation Oncology, Lineberger Comprehensive Cancer Center, University of North Carolina at Chapel Hill, Chapel Hill, USA

[Δ]Department of Radiology and Biomedical Research Imaging Center, University of North Carolina at Chapel Hill, Chapel Hill, NC, USA

[#] These authors contributed equally to this work.

Abstract

Using X-ray as the irradiation source, a photodynamic therapy process can be initiated from under deep tissues. This technology, referred to as X-ray induced PDT, or X-PDT, holds great potential to treat tumors at internal organs. To this end, one question is how to navigate the treatment to tumors with accuracy with external irradiation. Herein we address the issue with a novel, $LiGa_5O_8$: Cr (LGO:Cr)-based nanoscintillator, which emits persistent, near-infrared X-ray luminescence. This permits deep-tissue optical imaging that can be employed to guide irradiation. Specifically, we encapsulated LGO:Cr nanoparticles and a photosensitizer, 2,3-naphthalocyanine, into mesoporous silica nanoparticles. The nanoparticles were conjugated with cetuximab and systemically injected into H1299 orthotopic non-small cell lung cancer tumor models. The nanoconjugates can efficiently home to tumors in the lung, confirmed by monitoring X-ray luminescence from LGO:Cr. Guided by the imaging, external irradiation was applied, leading to efficient tumor suppression while minimally affecting normal tissues. To the best of our knowledge, the present study is the first to demonstrate, with systematically injected nanoparticles,

[*]**Corresponding Author**: shenbzh@vip.sina.com. jinxie@uga.edu.

Author Contributions

The manuscript was written through contributions of all authors. All authors have given approval to the final version of the manuscript.

Supporting Information. The Supporting Information is available.

that X-PDT can suppress growth of deep-seated tumors. The imaging guidance is also new to X-PDT, and is significant to the further transformation of the technology.

Graphical Abstract

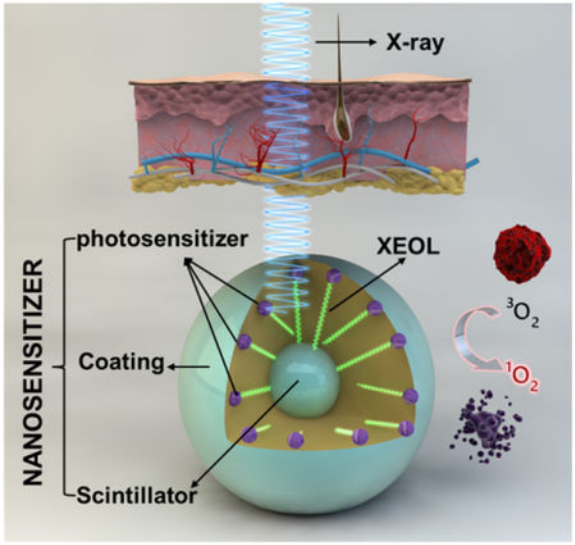

$LiGa_5O_8$:Cr nanoparticles mediate near-infrared X-ray luminescence and X-ray induced photodynamic therapy, making them attractive theranostic agents for cancer therapy.

Keywords

Nanomedicine; X-ray excited optical luminescence; photodynamic therapy; nanotheranostics; non-small cell lung cancer

Photodynamic therapy (PDT) is a relatively new cancer treatment modality.[1–3] PDT utilizes light reactive molecules called photosensitizers which, when exposed to light of proper wavelengths, produce cytotoxic reactive oxygen species (ROS). PDT can suppress tumor growth by directly killing cancer cells, damaging tumor-associated microvessels, or stimulating anti-tumor immune response.[2, 4–5] The treatment modality is minimally invasive, induces low systematic toxicity, and incurs little cumulative toxicity.[6–8] Despite of these advantages, the applications of PDT in the clinic have been limited. This is in large part attributed to the shallow tissue penetration (< 1 cm) of visible light and hence the inability of PDT to treat tumors at internal organs. Taking lung cancer for instance, PDT is not viable to treat the disease with external irradiation. There have been some successes on using bronchoscopic PDT to treat non-small cell lung cancer (NSCLC).[9–11] The approach, however, is limited by the tumor location, size, and foci number.

Several groups have recently reported on X-ray induced PDT, or X-PDT (Table S1). A central component of this technology is an integrated nanosystem that we call X-ray nanosensitizer. Each X-ray nanosensitizer (abbreviated as nanosensitizer henceforth) consists of a nanoparticle scintillator core, and is loaded with photosensitizer molecules

whose excitation matches the emission of the scintillator. Upon X-ray irradiation, the nanoscintillator converts X-ray photons to visible photons, a phenomenon known as X-ray excited optical luminescence (XEOL);[12–14] this is followed by activation of the photosensitizer in the nanosystem, leading to production of ROS, most importantly singlet oxygen ($^1O_2$). Because X-ray affords much greater tissue penetration capacity, this approach holds great potential in breaking the shallow penetration dogma.[15–16] The theory was first proposed by Chen et al.[17] and the feasibility was demonstrated *in vitro* with ZnS:Ag, CeF_3, TiO_2, and CdSe.[18] Later, other types of nanoscintillators, including those made of Y_2O_3, GdO_2S:Tb, LaF_3:Ce, ZnS:Cu,Co, and CeF_3,[19–28] have also been prepared and investigated *in vitro*. Very recently, we and others demonstrated the efficacy of approach in small animal models.[29–32] So far, however, all the *in vivo* studies were conducted in subcutaneous tumor models with intratumorally injected nanosensitizers. Bringing this technology forward, it is paramount to investigate whether systematically administered nanosensitizers can efficiently accumulate in tumors to mediate X-PDT. It is important that the assessment to be conducted in more clinically relevant tumor models. It demands that an imaging component to be included in the therapy so that irradiation can be delivered to tumors with high accuracy and at the best time interval. Currently, there have been few explorations along these directions.

We herein report 2,3-naphthalocyanine (NC) and $LiGa_5O_8$:Cr (LGO:Cr) co-loaded mesoporous silica nanoparticles (NC-LGO:Cr@$mSiO_2$) as a novel type of nanosensitizer. NC-LGO:Cr@$mSiO_2$ nanoparticles can efficiently mediate X-PDT, producing $^1O_2$ and killing cancer cells. On the other hand, unlike previously investigated scintillators,[28, 30, 32] whose XEOL peaks lie in the visible spectrum window, LGO:Cr emits strong XEOL at ~ 720 nm. More interestingly, the XEOL of LGO:Cr is persistent, lasting for minutes or even hours after the end of irradiation. The unique NIR and afterglow properties render LGO:Cr-based imaging with good tissue penetration, low luminescence background, and, as a result, deep tissue detection capacity. We showed that when conjugated with cetuximab (CTX), an anti-epidermal growth factor receptor (EGFR) antibody, the LGO:Cr nanoparticles can go through intravenous (i.v.) administration and hone to NSCLC tumors implanted into the lung of rodent models. Excitingly, we were able to monitor the accumulation event by LGO:Cr-mediated XEOL and employ the information to guide external X-ray irradiation to focus on tumors while sparing most normal tissues. While we previously studied LGO:Cr-based optical stimulated persistent luminescence,[33–34] there has been no report on utilizing the material for scintillation and X-PDT purposes. The imaging-guidance feature and the use of orthotopic NSCLC models are new to the X-PDT investigation and represent an important advance in the methodology transformation.

Synthesis and characterization of LGO:Cr@$mSiO_2$ nanoparticles

LGO:Cr nanoparticles were prepared using a polystyrene sphere-assisted sol-gel method.[34] Briefly, lithium nitrate, gallium nitrate and chromium nitrate were dissolved in water and mixed with acetylacetone, ammonium and polystyrene spheres to form a homogeneous sol. The sol was heated at 80 °C, and the resulting dry gel was calcined in the air at 1000–1100 ˚C for 3–5 h. The composition of the resulting material was determined by inductively coupled plasma (ICP) as $LiGa_5O_8$, with ~1wt% Cr dopant. X-ray diffraction (XRD) also confirmed that the material was spinel phase $LiGa_5O_8$ (JSPDF No. 76–199, Figure 1a).[34–36]

Followed by mechanically grounding, sedimentation, filtration and centrifugation, LGO:Cr nanoparticles can be obtained with small sizes (Figure 1b). These nanoparticles were subsequently coated with a layer of mesoporous silica by following a published protocol.[30] Both tetraethyl orthosilicate (TEOS) and (3-aminopropyl)triethoxysilane (APTES) were used as silane precursors so that the nanoparticles possess multiple amine groups on the surface. Transmission electron microscopy (TEM) found that the resulting LGO:Cr@$mSiO_2$ particles had a LGO:Cr core size of 100.9 ± 31.7 nm (Figure 1b) and a silica coating thickness of 25.6 ± 2.5 nm (Figure 1c). For good colloidal stability, we then PEGylated the nanoparticles by conjugating NHS-PEG-COOH (m.w. = 5000) to the surface. The resulting nanoparticles are stable in aqueous solutions (Figure S1; referred to as PEG-LGO:Cr@$mSiO_2$ for simplicity).

Optical properties of LGO:Cr@$mSiO_2$ nanoparticles

LGO:Cr@$mSiO_2$ nanoparticles can be excited by X-ray to emit intense NIR luminescence centered on ~720 nm (Figure 1d, S2). Such XEOL emission is attributed to the spin-forbidden $^2E \rightarrow {}^4A_2$ transition of Cr^{3+}, which was observed previously by us with bulk LGO:Cr under UV irradiation.[33–34] The XEOL can not only be detected on a fluorescene spectrometer, but also on a bio-imaging scanner, for instance an IVIS system (Figure 1e). Interestingly, the XOEL has a long life-time. For instance, when 0.2 mg LGO:Cr@$mSiO_2$ nanoparticles were irradiated by X-ray (50 kV, 0.02 Gy), the material emitted persistent luminescence that can be visualized by IVIS in the bioluminescence (BLI) mode, minutes or even hours after the conclusion of irradiation (Figure 1e). Moreover, decayed LGO:Cr nanoparticles could be re-stimulated after short exposure to X-ray (Figure 1e,f), and repeated stimulation did not weaken the luminescence intensity (Figure S3). These properties suggest great potential of employing the XEOL of LGO:Cr for imaging.

For conventional fluorescence imaging, a major drawback is the skin autofluorescence. Autofluorescence becomes overwhelming when fluorophors of interest are located more than 1 cm beneath the skin, making deep-tissue imaging challenging or not possible.[37] For LGO:Cr-based XEOL, however, background signal is expected to be at the minimum since irradiation is ceased at detection. Such a hypothesis was first tested with LGO:Cr@$mSiO_2$ nanoparticles (0.8 mg) lain under a 1.5-cm-thick pork slice (Figure 2a). Despite thick tissues, XEOL can be efficiently stimulated (1.52×10^9 p/s/cm^2/sr with 0.02 Gy X-ray through 1.5-cm pork and 3.17×10^9 p/s/cm^2/sr with 0.1 Gy X-ray; the tissue slice was removed before imaging, Figure 2a). Such luminescence was readily detected from under 1.5-cm pork (Figure 2b), which is not possible with fluorescence.[38–39] Such XEOL can be repeatedly stimulated without losing signal intensity (Figure 2b,c).

The tissue penetration was further investigated *in vivo*. Briefly, we intramuscularly injected LGO:Cr@$mSiO_2$ nanoparticles (0.2 mg in 0.2 mL PBS) into the hind leg of an athymic nude mouse from the prone position. The animal was then flipped, and X-ray (0.02 Gy) was applied to the injected sites, but from the supine position. We then performed imaging (in the BLI mode) either immediately after the irradiation or 5 and 10 minutes apart. We found that from under bones and thick tissues, LGO:Cr@$mSiO_2$ can be activated to emit strong and durable luminescence (>10^9 p/s/cm^2/sr, Figure 3a,b). In addition, because of minimal

background, such XEOL-based imaging affords great signal-to-noise ratios (Table S2). The imaging quality is not compromised over repeated stimulations (Figure 3b). Overall, these results further confirm the advantages of LGO:Cr-mediated XEOL as a means for small animal imaging.[40]

NC-LGO:Cr@mSiO$_2$-mediated X-PDT

We next examined whether LGO:Cr@mSiO$_2$ can be employed to activate X-PDT. For this purpose, we loaded NC, a photosensitizer (maximum excitation wavelength of 712 nm[41–42]), into the mesoporous layer of LGO:Cr@mSiO$_2$ (2 wt%) to match the emission of LGO:Cr (Figure 4a). The resulting nanoparticles are stable in aqueous solutions and PBS (Fig. S1). To assess $^1O_2$ production, the resulting NC-LGO:Cr@mSiO$_2$ nanoparticles (0.05 mg/mL) were incubated with singlet oxygen sensor green (SOSG) in a PBS solution in a quartz cell. X-ray of different doses (0–4 Gy) was applied to the solution, and the 525-nm emission of SOSG was monitored (Figure 4b). X-ray alone induced minimal increase of luminescence, so did NC plus X-ray and LGO:Cr@mSiO$_2$ plus X-ray. NC-LGO:Cr@mSiO$_2$, on the other hand, led to a significant, time-dependent increase of fluorescence intensity, suggesting efficient production of $^1O_2$ by X-PDT (Figure 4b). Based on the readings, it was estimated that the $^1O_2$ production efficiency (η) is 1.26% (Table S3, detailed in the Supporting Information).[31]

The $^1O_2$ production was also analyzed *in vitro* with H1299 cells, which are a human NSCLC cell line.[43] Briefly, NC-LGO:Cr@mSiO$_2$ nanoparticles (50 μg/mL) were first incubated with H1299 cells for 2 h, after which the medium was replenished with a fresh one that contained 5 μM SOSG. This was followed by X-ray irradiation (4 Gy) and microscopic imaging. Consistent with the observations in solutions, X-PDT (NC-LGO:Cr@mSiO$_2$ plus X-ray) led to a significant increase of $^1O_2$ levels in cells (Figure 4c). As a comparison, when the cells were treated with LGO:Cr@mSiO$_2$ plus X-ray or X-ray only, there was no detectable increase of SOSG signals (Figure 4c). These results confirm that it takes the combination of NC, LGO:Cr@mSiO$_2$, and X-ray to produce $^1O_2$.

X-PDT to kill cancer cells

Cell viability was studied with H1299 cells using both ethidium homodimer-1 staining (Ethd-1, which is a cell-impermeant viability indicator) and MTT assay. For Ethd-1 staining, we found that NC-LGO:Cr@mSiO$_2$ nanoparticles (50 μg/mL) plus X-ray irradiation (4 Gy) led to extensive cell death, manifested in an increased level of red fluorescence in cells (Figure 5a). As a comparison, cells treated by NC-LGO:Cr@mSiO$_2$ alone or X-ray alone caused no significant change of red fluorescence (Figure 5a). Similar observation was made with MTT assays. When cells were treated with NC-LGO:Cr@mSiO$_2$ nanoparticles alone (0–0.1 mg/mL, Figure S4) and X-rays alone (0–6 Gy, Figure 5b), there was no detectable cell viability drop at 24 hrs. With the combination (i.e. X-PDT), on the other hand, the treatment led to efficient cell death (Figure 5b). For instance, when 50 μg/mL of NC-LGO:Cr@mSiO$_2$ and 2 Gy irradiation was applied, the cell viability was reduced to 46.4 ± 7.4%. It is noted that H1229 cells are refractory to radiotherapy,[44–46] and that ionizing radiation often induces not immediate cell death but reduced reproductive capacity that

would manifest in days or weeks.[47] The viability drop by X-PDT but not X-ray alone at 24 hrs, therefore, suggests a different, PDT related mechanism of cell death.

Such X-PDT-induced cytotoxicity can be activated from beneath thick tissues. This was confirmed by repeating the preceding MTT assays but with pork slices lain between X-ray source and cells. X-PDT (NC-LGO:Cr@$mSiO_2$ 50 μg/mL, 2 Gy X-ray) was able to efficiently kill H1299 cells, reducing the viability to 50.2 ± 3.4% and 60.1 ± 1.7% at a pork thickness of 1.6 cm and 2.8 cm, respectively (Figure 5c). These results were comparable to those without pork, suggesting relatively small impact of the tissue depth on treatment efficacy (46.4 ± 7.4%, Figure 5b).

Cetuximab conjugated NC-LGO:Cr@$mSiO_2$ for tumor targeting

To ensure selective tumor eradication, it is essential that both nanosensitizers and radiation are navigated to tumors with high accuracy. To this end, we conjugated cetuximab to the carboxyl groups on the particle surface using EDC/NHS chemistry.[48] The conjugation was confirmed by Fourier transform infrared spectroscopy (FT-IR, Fig. S5) and Coomassie blue (Bradford) protein assay (Fig. S6). Cetuximab-conjugated NC-LGO:Cr@$mSiO_2$ (i.e. NC-LGO:Cr@$mSiO_2$-CTX) showed excellent stability in water and PBS solution (Figure S7). Moreover, due to relative hydrophobicity of NC molecules, there was limited leakage of the photosensitizer in aqueous surroundings (Figure S8).

Cetuximab targets EGFR, which is up-regulated in many types of cancer.[49–50] In particular, EGFR is overexpressed in many patients with NSCLC, including 39% in adenocarcinoma, 58% in squamous cell carcinoma, and 38% in large cell carcinoma.[51] To study targeting specificity, we incubated NC-LGO:Cr@$mSiO_2$-CTX with H1299 cells, which are EGFR-positive.[49] Microscopic imaging found efficient internalization of the nanoparticles (Figure 6a, 0.05 mg/mL); as a comparison, NC-LGO:Cr@$mSiO_2$ nanoparticles showed minimal cell uptake (Figure 6a). Notably, MTT assay found that there was no detectable cytotoxicity with NC-LGO:Cr@$mSiO_2$-CTX in the dark in this concentration range (Fig. S9).

We further studied the targeting specificity *in vivo* with an orthotopic lung tumor model established with H1299 cells. Briefly, the animal models were established by percutaneously injecting H1299-luc cells in 50 μL of matrigel into the lateral thorax at the lateral dorsal axillary line of a nude mouse. The cells had been transfected with firefly luciferase (f-luc), so we can track the tumor growth using BLI. Fourteen days after the inoculation, NC-LGO:Cr@$mSiO_2$-CTX or NC-LGO:Cr@$mSiO_2$ were i.v. injected into the animals (n = 3, 0.4 mg per mouse). At selective time points, the chest area was exposed to short X-ray irradiation (0.02 Gy), and the animals were immediately imaged on an IVIS scanner. For animals injected with NC-LGO:Cr@$mSiO_2$-CTX, strong signals were observed in the lung areas (Figure 6b), which was attributed to cetuximab-mediated tumor uptake. The peak signals (1.96×10^8 p/s/cm^2/sr) were observed at 4 h (Figure 6c). In the control group, much lower tumor uptake was observed at all time points (e.g. 2.67×10^4 p/s/cm^2/sr at 4 h). After the 24 h imaging, the animals were euthanized. *Ex vivo* imaging confirmed the high tumor uptake of NC-LGO:Cr@$mSiO_2$-CTX (8.16×10^8 p/s/cm^2/sr), but not NC-LGO:Cr@$mSiO_2$ nanoparticles (8.70×10^4 p/s/cm^2/sr), as shown in Figure 6d,e.

XEOL-guided X-PDT for lung cancer treatment

The therapy study was also conducted with the H1299 orthotopic tumor model. NC-LGO:Cr@mSiO_2-CTX nanoparticles were first i.v. injected (n = 6, 10 mg/kg). Four hours after the injection, X-ray (0.02 Gy) was applied to the lung area to stimulate XEOL. Based on the imaging results, the tumor areas were delineated and marked on the animal skin (Figure S10,11). After that, X-ray (6 Gy) was applied to the marked areas, with the rest of the body lead-shielded. In control groups, animals received PBS plus X-ray (6 Gy) or PBS only.

After the treatments, animals were subjected to BLI at different time points to monitor tumor growth. Region of interest (ROI) readings were recorded and compared between the therapy and control groups to assess the treatment efficacy. For the PBS control group, tumors grew rapidly, with the averaging ROI reading reaching 1.16×10^{10} p/s/cm^2/sr on day 7 (Figure 7a, b). Radiation alone had mediocre impact on tumor growth, showing an average reading of 5.82×10^9 p/s/cm^2/sr on Day 7. As a comparison, tumor growth was efficiently suppressed when treated with NC-LGO:Cr@mSiO_2-CTX plus radiation, with BLI readings of 3.98×10^8, 5.98×10^8, and 9.33×10^8 p/s/cm^2/sr on Day 1, 3, and 7, respectively (Figure 7a). This amounts to tumor inhibition rates of 3.43, 5.16, and 8.04%. Immediately after the imaging on Day 7, we euthanized the animals, dissected lungs from the thorax, and conducted BLI with the tissues. The residual f-luc signals confirmed the large difference between the X-PDT group and the X-ray only group (Figure S12). The BLI data also corroborated well with haematoxylin and eosin (H&E) staining resulting, finding many necrotic areas in the X-PDT group along with less tumor nodules and smaller tumor sizes (Figure 7c). Meanwhile, H&E staining with tissues from the adjacent organs, including the heart, liver, kidney, and spleen, found no detectable toxicity (Figure S13). This is attributed to imaging-guided irradiation that maximized the selectivity of the treatment and minimized damage to normal tissues.[52]

Discussions and Conclusion

Breaking the shallow penetration dogma of conventional PDT, X-PDT holds great potential in managing tumors in deep-tissues. So far, however, there have been few successful demonstrations with systematically injected nanoscintillators. One of the problems is the relatively large nanoparticle size (e.g. ~ 407 nm MC540-$SrAl_2O_4$:Eu@SiO_2,[30] ~20 μm Gd_2O_2S:Tb,[10b] and mircosize SiC/SiOx[10e]). In the current study, we were able to achieve good X-PDT efficiency with ~100 nm NC-LGO:Cr@mSiO_2. After PEGylation and conjugation with cetuximab, the nanoparticles were able to home efficiently to tumors implanted into the lung after i.v. injection.

The tumor selectivity is further enhanced by navigating X-ray irradiation to tumor areas with imaging-guidance. This is possible because LGO:Cr affords NIR and persistent luminescence and, as a result of it, deep tissue detection capacity. As a comparison, most previously investigated scintillator materials have their emission in the visible spectrum window (e.g. $SrAl_2O_4$:Eu, Gd_2O_2S:Tb, and SiC/SiOx). There have been extensive efforts on improving the penetration depth of light-mediated imaging and therapy,[53–62] and the current

approach echoes the endeavor. Interestingly, our studies found that the persistent XEOL of LGO:Cr is able to mediate X-PDT and cell killing after the conclusion of X-ray irradiation (Figure S14, S15). This may allow X-PDT to be activated by intermitted X-ray irradiation that can further ionizing-irradiation induced toxicity. This possibility will be investigated in future studies.

In summary, we have investigated LGO:Cr as a novel scintillator material for efficient X-PDT against NSCLC. Unlike previous scintillators, LGO:Cr affords NIR and persistent luminescence. This enables XEOL-based tracking of nanoparticles *in vivo* and imaging-guided irradiation during therapy. The resulting therapy is efficient and highly selective, causing minimal collateral damage. These advances are of great value to the development of X-PDT as a novel treatment modality.

Supplementary Material

Refer to Web version on PubMed Central for supplementary material.

ACKNOWLEDGMENT

This work was supported by the National Institutes of Health (R01EB022596, and R01NS093314), the Congressionally Directed Medical Research Program (CA140666), the National Science Foundation (NSF1552617), the University of Georgia–Georgia Regents University seed grant program, and the University of Georgia Postdoc Research Award program. We also thank the National Basic Research Program of China (2015CB931800), the National Natural Science Foundation of China (81130028, 31210103913, 81471724, 81101088), the Natural Science Foundation of Heilongjiang Province of China (LC2013C26), Innovation Fund Designated of Harbin (2014RFQGJ011), the Youth Science WU LIANDE Foundation of Harbin Medical University (WLD-QN1119), the Fourth Hospital of Harbin Medical University Fund for Distinguished Young Scholars, and the Key Laboratory of Molecular Imaging Foundation (College of Heilongjiang Province).

REFERENCES

1. Agostinis P; Berg K; Cengel KA; Foster TH; Girotti AW; Gollnick SO; Hahn SM; Hamblin MR; Juzeniene A; Kessel D; Korbelik M; Moan J; Mroz P; Nowis D; Piette J; Wilson BC; Golab J, Photodynamic Therapy of Cancer: An Update. Ca-Cancer J Clin 2011, 61 (4), 250–281. [PubMed: 21617154]
2. Castano AP; Mroz P; Hamblin MR, Photodynamic therapy and anti-tumour immunity. Nat Rev Cancer 2006, 6 (7), 535–545. [PubMed: 16794636]
3. Dolmans DEJGJ; Fukumura D; Jain RK, Photodynamic therapy for cancer. Nat Rev Cancer 2003, 3 (5), 380–387. [PubMed: 12724736]
4. Juarranz A; Jaen P; Sanz-Rodriguez F; Cuevas J; Gonzalez S, Photodynamic therapy of cancer. Basic principles and applications. Clin Transl Oncol 2008, 10 (3), 148–154. [PubMed: 18321817]
5. Lucky SS; Soo KC; Zhang Y, Nanoparticles in Photodynamic Therapy. Chem Rev 2015, 115 (4), 1990–2042. [PubMed: 25602130]
6. Lim CK; Heo J; Shin S; Jeong K; Seo YH; Jang WD; Park CR; Park SY; Kim S; Kwon IC, Nanophotosensitizers toward advanced photodynamic therapy of Cancer. Cancer Lett 2013, 334 (2), 176–187. [PubMed: 23017942]
7. Lovell JF; Liu TW; Chen J; Zheng G, Activatable photosensitizers for imaging and therapy. Chemical reviews 2010, 110 (5), 2839–57. [PubMed: 20104890]
8. Sharman WM; Allen CM; van Lier JE, Photodynamic therapeutics: basic principles and clinical applications. Drug discovery today 1999, 4 (11), 507–517. [PubMed: 10529768]
9. Mathur PN; Edell E; Sutedja T; Vergnon JM; American College of Chest, P., Treatment of early stage non-small cell lung cancer. Chest 2003, 123 (1 Suppl), 176S–180S. [PubMed: 12527577]

10. McCaughan JS Jr.; Williams TE Jr.; Bethel BH, Photodynamic therapy of endobronchial tumors. Lasers in surgery and medicine 1986, 6 (3), 336–45. [PubMed: 2942745]
11. Kato H; Harada M; Ichinose S; Usuda J; Tsuchida T; Okunaka T, Photodynamic therapy (PDT) of lung cancer: experience of the Tokyo Medical University. Photodiagnosis and photodynamic therapy 2004, 1 (1), 49–55. [PubMed: 25048064]
12. Dsilva AP; Fassel VA, Analytical Applications of X-Ray Excited Optical Luminescence - Direct Determination of Rare-Earth Nuclear Poisons in Zirconia. Anal Chem 1974, 46 (8), 996–999.
13. van Eijk CWE, Inorganic scintillators in medical imaging. Phys Med Biol 2002, 47 (8), R85–R106. [PubMed: 12030568]
14. Chen HY; Rogalski MM; Anker JN, Advances in functional X-ray imaging techniques and contrast agents. Phys Chem Chem Phys 2012, 14 (39), 13469–13486. [PubMed: 22962667]
15. Karnkaew A; Chen F; Zhan YH; Majewski RL; Cai WB, Scintillating Nanoparticles as Energy Mediators for Enhanced Photodynamic Therapy. Acs Nano 2016, 10 (4), 3918–3935. [PubMed: 27043181]
16. Hu J; Tang Y; Elmenoufy AH; Xu H; Cheng Z; Yang X, Nanocomposite-Based Photodynamic Therapy Strategies for Deep Tumor Treatment. Small 2015, 11 (44), 5860–87. [PubMed: 26398119]
17. Chen W; Zhang J, Using nanoparticles to enable simultaneous radiation and photodynamic therapies for cancer treatment. J Nanosci Nanotechno 2006, 6 (4), 1159–1166.
18. Takahashi J, M. M, Analysis of Potential Radiosensitizing Materials for X-Ray-Induced Photodynamic Therapy. NanoBiotechnology 2007, 3 (2), 116.
19. Scaffidi JP; Gregas MK; Lauly B; Zhang Y; Vo-Dinh T, Activity of Psoralen-Functionalized Nanoscintillators against Cancer Cells upon X-ray Excitation. Acs Nano 2011, 5 (6), 4679–4687. [PubMed: 21553850]
20. Abliz E; Collins JE; Bell H; Tata DB, Novel applications of diagnostic X-rays in activating a clinical photodynamic drug: Photofrin II through X-ray induced visible luminescence from “rare-earth” formulated particles. Journal of X-ray science and technology 2011, 19 (4), 521–530. [PubMed: 25214384]
21. Zou XJ; Yao MZ; Ma L; Hossu M; Han XM; Juzenas P; Chen W, X-ray-induced nanoparticle-based photodynamic therapy of cancer. Nanomedicine-Uk 2014, 9 (15), 2339–2351.
22. Ma L; Zou XJ; Bui B; Chen W; Song KH; Solberg T, X-ray excited ZnS:Cu,Co afterglow nanoparticles for photodynamic activation. Appl Phys Lett 2014, 105 (1), 013702.
23. Rossi F; Bedogni E; Bigi F; Rimoldi T; Cristofolini L; Pinelli S; Alinovi R; Negri M; Dhanabalan SC; Attolini G; Fabbri F; Goldoni M; Mutti A; Benecchi G; Ghetti C; Iannotta S; Salviati G, Porphyrin conjugated SiC/SiOx nanowires for X-ray-excited photodynamic therapy. Sci Rep-Uk 2015, 5, 7606.
24. Kascakova S; Giuliani A; Lacerda S; Pallier A; Mercere P; Toth E; Refregiers M, X-ray-induced radiophotodynamic therapy (RPDT) using lanthanide micelles: Beyond depth limitations. Nano Res 2015, 8 (7), 2373–2379.
25. Generalov R; Kuan WB; Chen W; Kristensen S; Juzenas P, Radiosensitizing effect of zinc oxide and silica nanocomposites on cancer cells. Colloid Surface B 2015, 129, 79–86.
26. Homayoni H; Jiang K; Zou XJ; Hossu M; Rashidi LH; Chen W, Enhancement of protoporphyrin IX performance in aqueous solutions for photodynamic therapy. Photodiagn Photodyn 2015, 12 (2), 258–266.
27. Clement S; Deng W; Camilleri E; Wilson BC; Goldys EM, X-ray induced singlet oxygen generation by nanoparticle-photosensitizer conjugates for photodynamic therapy: determination of singlet oxygen quantum yield. Sci Rep-Uk 2016, 6, 19954.
28. Tang YG; Hu J; Elmenoufy AH; Yang XL, Highly Efficient FRET System Capable of Deep Photodynamic Therapy Established on X-ray Excited Mesoporous LaF3:Tb Scintillating Nanoparticles. Acs Appl Mater Inter 2015, 7 (22), 12261–12269.
29. Ma L; Zou XJ; Chen W, A New X-Ray Activated Nanoparticle Photosensitizer for Cancer Treatment. J Biomed Nanotechnol 2014, 10 (8), 1501–1508. [PubMed: 25016650]

30. Chen H; Wang GD; Chuang YJ; Zhen Z; Chen X; Biddinger P; Hao Z; Liu F; Shen B; Pan Z; Xie J, Nanoscintillator-mediated X-ray inducible photodynamic therapy for in vivo cancer treatment. Nano letters 2015, 15 (4), 2249–56. [PubMed: 25756781]

31. Zhang C; Zhao KL; Bu WB; Ni DL; Liu YY; Feng JW; Shi JL, Marriage of Scintillator and Semiconductor for Synchronous Radiotherapy and Deep Photodynamic Therapy with Diminished Oxygen Dependence. Angew Chem Int Edit 2015, 54 (6), 1770–1774.

32. Wang GD, N. HT, Chen H, Cox PB, Wang L, Nagata K, Hao Z, Wang A, Li Z, Chen H, Xie J, X-Ray Induced Photodynamic Therapy: A Combination of Radiotherapy and Photodynamic Therapy. Theranostics 2016, 6(13):2295–2305. [PubMed: 27877235]

33. Liu F; Yan WZ; Chuang YJ; Zhen ZP; Xie J; Pan ZW, Photostimulated near-infrared persistent luminescence as a new optical read-out from Cr3+-doped LiGa5O8. Sci Rep-Uk 2013, 3, 1554.

34. Chuang YJ; Zhen ZP; Zhang F; Liu F; Mishra JP; Tang W; Chen HM; Huang XL; Wang LC; Chen XY; Xie J; Pan ZW, Photostimulable Near-Infrared Persistent Luminescent Nanoprobes for Ultrasensitive and Longitudinal Deep-Tissue Bio-Imaging. Theranostics 2014, 4 (11), 1112–1122. [PubMed: 25285164]

35. Abdukayum A; Chen JT; Zhao Q; Yan XP, Functional near infrared-emitting Cr3+/Pr3+ co-doped zinc gallogermanate persistent luminescent nanoparticles with superlong afterglow for in vivo targeted bioimaging. Journal of the American Chemical Society 2013, 135 (38), 14125–33. [PubMed: 23988232]

36. Golubev NV; Ignat'eva ES; Sigaev VN; Lauria A; De Trizio L; Azarbod A; Paleari A; Lorenzi R, Diffusion-driven and size-dependent phase changes of gallium oxide nanocrystals in a glassy host. Physical chemistry chemical physics : PCCP 2015, 17 (7), 5141–50. [PubMed: 25599651]

37. Massoud TF; Gambhir SS, Molecular imaging in living subjects: seeing fundamental biological processes in a new light. Genes & development 2003, 17 (5), 545–80. [PubMed: 12629038]

38. Kosaka N; Ogawa M; Choyke PL; Kobayashi H, Clinical implications of near-infrared fluorescence imaging in cancer. Future oncology 2009, 5 (9), 1501–11. [PubMed: 19903075]

39. Leblond F; Davis SC; Valdes PA; Pogue BW, Pre-clinical whole-body fluorescence imaging: Review of instruments, methods and applications. Journal of photochemistry and photobiology. B, Biology 2010, 98 (1), 77–94.

40. Berezin MY; Achilefu S, Fluorescence lifetime measurements and biological imaging. Chem Rev 2010, 110 (5), 2641–84. [PubMed: 20356094]

41. Song LP; Li H; Sunar U; Chen J; Corbin I; Yodh AG; Zheng G, Naphthalocyanine-reconstituted LDL nanoparticles for in vivo cancer imaging and treatment. Int J Nanomed 2007, 2 (4), 767–774.

42. Ali H; van Lier JE, Metal complexes as photo- and radiosensitizers. Chem Rev 1999, 99 (9), 2379–2450. [PubMed: 11749485]

43. Hong M; Ren MQ; Silva J; Kennedy T; Choi J; Cowell JK; Hao ZL, Sepantronium is a DNA damaging agent that synergizes with PLK1 inhibitor volasertib. Am J Cancer Res 2014, 4 (2), 135–147. [PubMed: 24660103]

44. Sung HY; Wu HG; Ahn JH; Park WY, Dcr3 inhibit p53-dependent apoptosis in gamma-irradiated lung cancer cells. Int J Radiat Biol 2010, 86 (9), 780–790. [PubMed: 20597837]

45. Kim EH; Park AK; Dong SM; Ahn JH; Park WY, Global analysis of CpG methylation reveals epigenetic control of the radiosensitivity in lung cancer cell lines. Oncogene 2010, 29 (33), 4725–4731. [PubMed: 20531302]

46. Im CN; Kim BM; Moon EY; Hong DW; Park JW; Hong SH, Characterization of H460R, a Radioresistant Human Lung Cancer Cell Line, and Involvement of Syntrophin Beta 2 (SNTB2) in Radioresistance. Genomics & informatics 2013, 11 (4), 245–53. [PubMed: 24465237]

47. Gunderson LL; Tepper JE; Bogart JA, Clinical radiation oncology. 3rd ed.; Saunders/Elsevier: Philadelphia, Pa.; London, 2012; p xxiii, 1638 p.

48. Fischer MJE, Amine Coupling Through EDC/NHS: A Practical Approach. Methods Mol Biol 2010, 627, 55–73. [PubMed: 20217613]

49. Wong SF, Cetuximab: an epidermal growth factor receptor monoclonal antibody for the treatment of colorectal cancer. Clinical therapeutics 2005, 27 (6), 684–94. [PubMed: 16117976]

50. Galizia G; Lieto E; De Vita F; Orditura M; Castellano P; Troiani T; Imperatore V; Ciardiello F, Cetuximab, a chimeric human mouse anti-epidermal growth factor receptor monoclonal antibody,

in the treatment of human colorectal cancer. Oncogene 2007, 26 (25), 3654–60. [PubMed: 17530019]

51. Lee SM, Is EGFR expression important in non-small cell lung cancer? Thorax 2006, 61 (2), 98–99. [PubMed: 16443704]
52. Cui YH; Suh Y; Lee HJ; Yoo KC; Uddin N; Jeong YJ; Lee JS; Hwang SG; Nam SY; Kim MJ; Lee SJ, Radiation promotes invasiveness of non-small-cell lung cancer cells through granulocyte-colony-stimulating factor. Oncogene 2015, 34 (42), 5372–82. [PubMed: 25639867]
53. Idris NM; Gnanasammandhan MK; Zhang J; Ho PC; Mahendran R; Zhang Y, In vivo photodynamic therapy using upconversion nanoparticles as remote-controlled nanotransducers. Nature medicine 2012, 18 (10), 1580–U190.
54. Gu Z; Yan L; Tian G; Li S; Chai Z; Zhao Y, Recent advances in design and fabrication of upconversion nanoparticles and their safe theranostic applications. Adv Mater 2013, 25 (28), 3758–79. [PubMed: 23813588]
55. Chen G; Qiu H; Prasad PN; Chen X, Upconversion nanoparticles: design, nanochemistry, and applications in theranostics. Chem Rev 2014, 114 (10), 5161–214. [PubMed: 24605868]
56. Naczynski DJ; Sun C; Turkcan S; Jenkins C; Koh AL; Ikeda D; Pratx G; Xing L, X-ray-induced shortwave infrared biomedical imaging using rare-earth nanoprobes. Nano letters 2015, 15 (1), 96–102. [PubMed: 25485705]
57. Sun C; Pratx G; Carpenter CM; Liu HG; Cheng Z; Gambhir SS; Xing L, Synthesis and Radioluminescence of PEGylated Eu3+-doped Nanophosphors as Bioimaging Probes. Adv Mater 2011, 23 (24), H195–H199. [PubMed: 21557339]
58. Moore TL; Wang FL; Chen HY; Grimes SW; Anker JN; Alexis F, Polymer-Coated Radioluminescent Nanoparticles for Quantitative Imaging of Drug Delivery. Adv Funct Mater 2014, 24 (37), 5815–5823.
59. Wang FL; Raval Y; Chen HY; Tzeng TRJ; DesJardins JD; Anker JN, Development of Luminescent pH Sensor Films for Monitoring Bacterial Growth Through Tissue. Adv Healthc Mater 2014, 3 (2), 197–204. [PubMed: 23832869]
60. Chen HY; Qi B; Moore T; Colvin DC; Crawford T; Gore JC; Alexis F; Mefford OT; Anker JN, Synthesis of Brightly PEGylated Luminescent Magnetic Upconversion Nanophosphors for Deep Tissue and Dual MRI Imaging. Small 2014, 10 (1), 160–168. [PubMed: 23828629]
61. Chen H; Moore T; Qi B; Colvin DC; Jelen EK; Hitchcock DA; He J; Mefford OT; Gore JC; Alexis F; Anker JN, Monitoring pH-Triggered Drug Release from Radioluminescent Nanocapsules with X-ray Excited Optical Luminescence. Acs Nano 2013, 7 (2), 1178–1187. [PubMed: 23281651]
62. Chen HY; Longfield DE; Varahagiri VS; Nguyen KT; Patrick AL; Qian HJ; VanDerveer DG; Anker JN, Optical imaging in tissue with X-ray excited luminescent sensors. Analyst 2011, 136 (17), 3438–3445. [PubMed: 21695291]

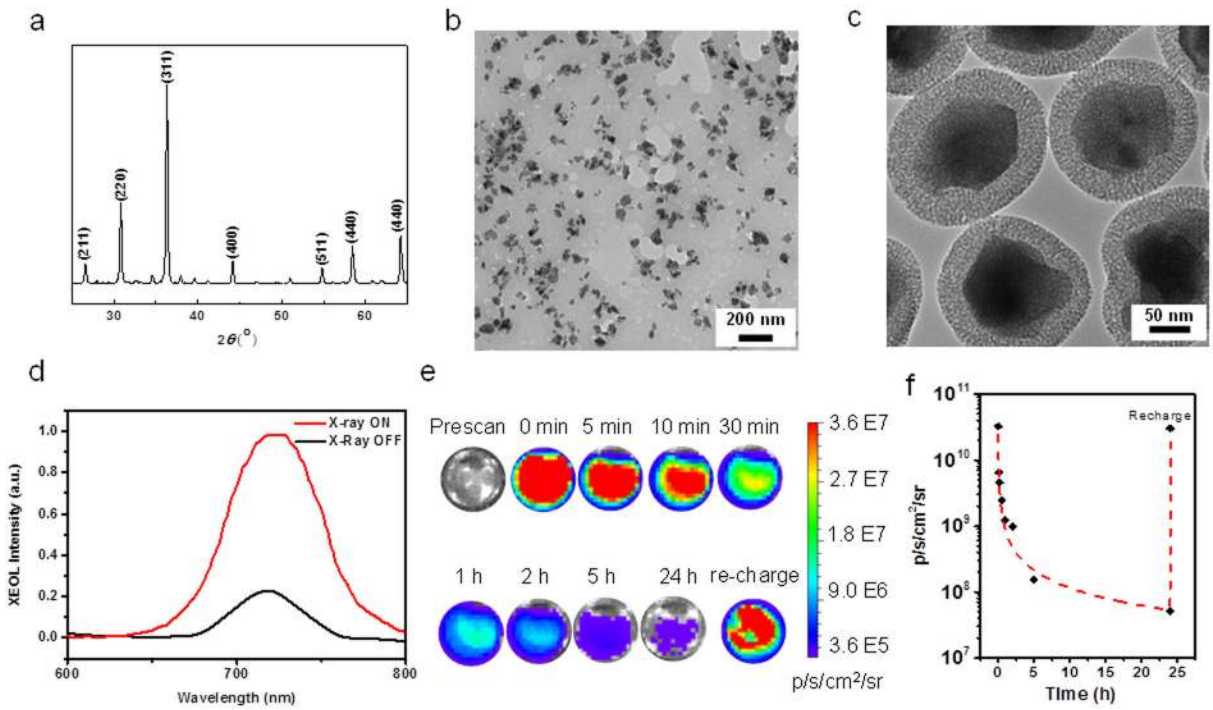

Figure 1.

Compositional and optical characterizations of LGO:Cr nanoparticles. a) XRD spectrum of LGO:Cr. b) TEM image of LGO:Cr nanoparticles. c) TEM image of LGO:Cr@mSiO$_2$ nanoparticles. d) XEOL of LGO:Cr@mSiO$_2$ nanoparticles. e) LGO:Cr@mSiO$_2$ phantom images, based on XEOL and recorded on an IVIS scanner in the BLI mode. f) Time-dependent XEOL intensity change, based on results from d).

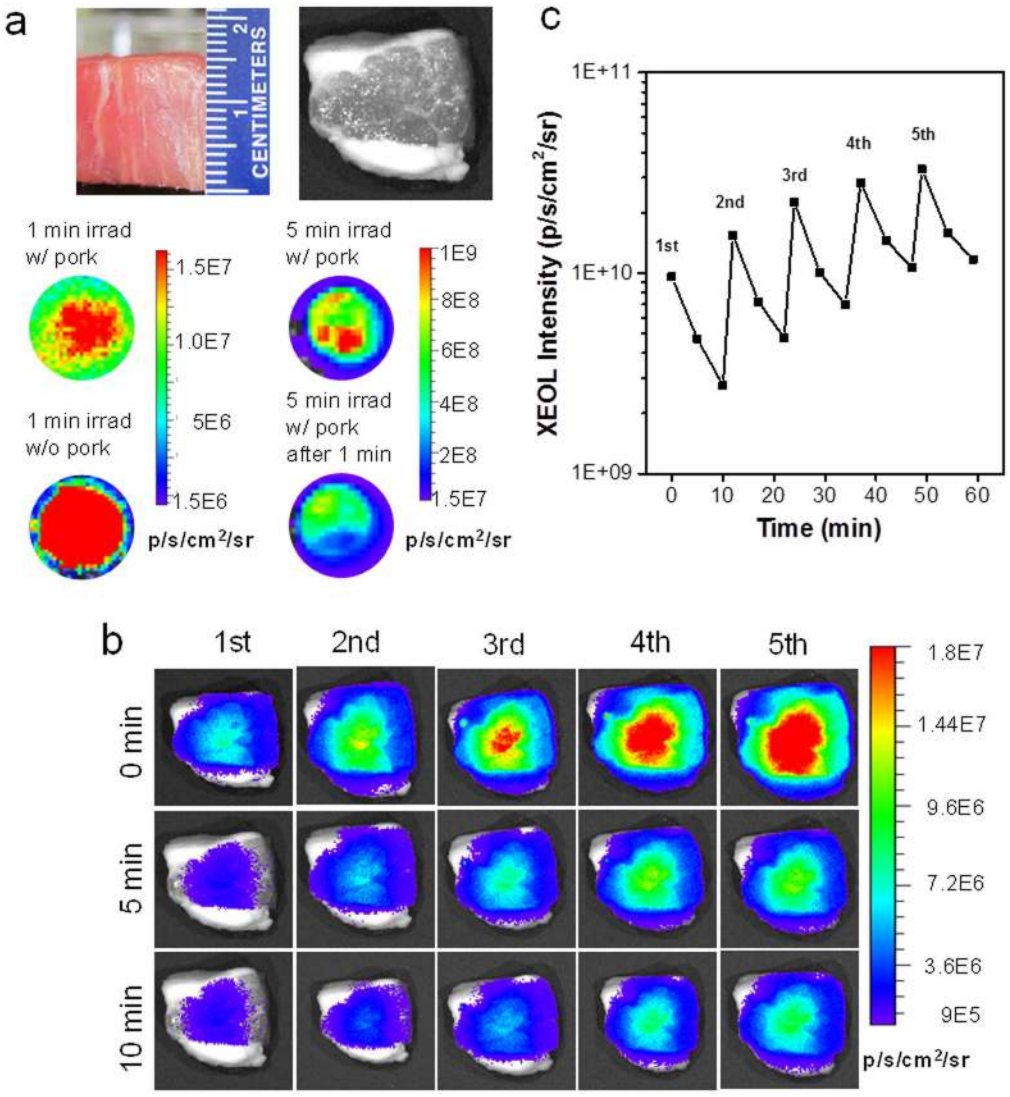

Figure 2.

XEOL imaging from beneath deep tissues using LGO:Cr nanoparticles. a) Stimulation of XEOL from under 1.5-cm thick pork. Pork slice was put on top of the particles during X-ray irradiation but removed during imaging. Left: afterglow images taken 1 min after X-ray irradiation. Right: afterglow images taken 5 min after X-ray irradiation. b) XEOL can be detected from under 1.5-cm thick pork. The images were acquired immediately after as well as 5 min and 10 min after X-ray exposure. The pork slice was remained on top of the particles throughout the experiment. c) XEOL intensity changes, based on BLI imaging results from b).

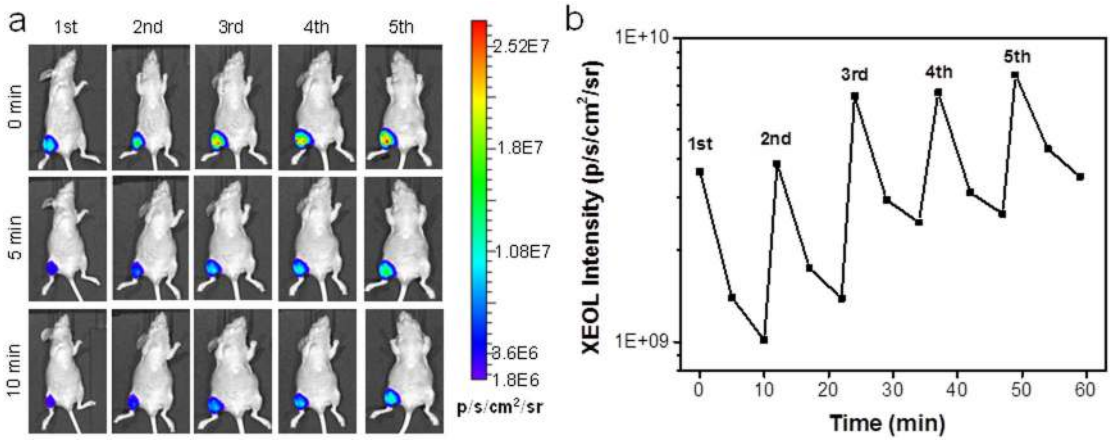

Figure 3.

In vivo XEOL imaging with intramuscularly injected LGO:Cr@mSiO$_2$ nanoparticles. The nanoparticles (0.2 mL, 1 mg/mL) were intramuscularly injected into the hind leg at the prone position; the X-ray stimulation and imaging were performed at the supine position. a) *In vivo* images, taken immediately after as well as 5 and 10 min after X-ray irradiation. XEOL can be repeatedly stimulated and the signals can be detected from beneath the mouse body. b) Changes of XEOL intensity, based on imaging results from (a).

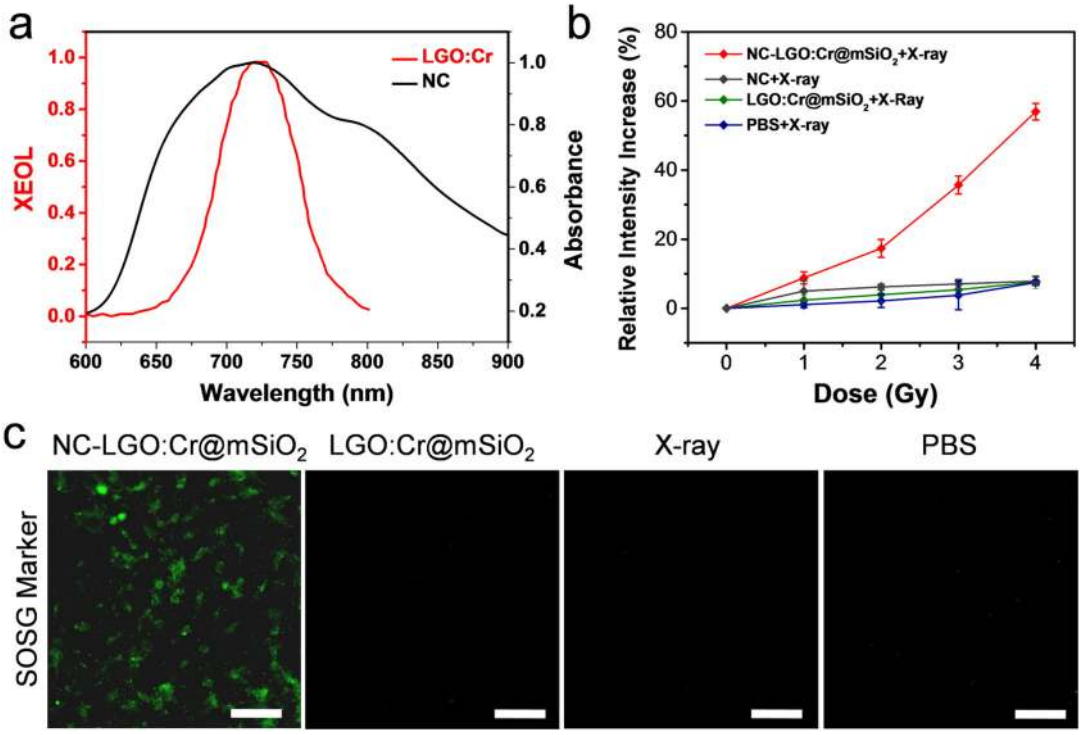

Figure 4.

$^1O_2$ production under X-ray irradiation using LGO:Cr nanoparticles as nanotransducers. a) Absorption spectrum of NC (black) and XEOL spectrum of LGO:Cr (red). Both spectra peaked at ~720 nm. b) $^1O_2$ production, measured by SOSG assay. NC-LGO:Cr@mSiO_2 efficiently produces $^1O_2$ under X-ray irradiation, manifested as increased 525-nm fluorescence. As a comparison, there was almost no $^1O_2$ produced in the controls. c) *In vitro* SOSG assay with H1299 cells. Efficient $^1O_2$ was produced within cells when X-ray was applied following cell incubation with NC-LGO:Cr@mSiO_2 nanoparticles. Scale bars, 100 μm.

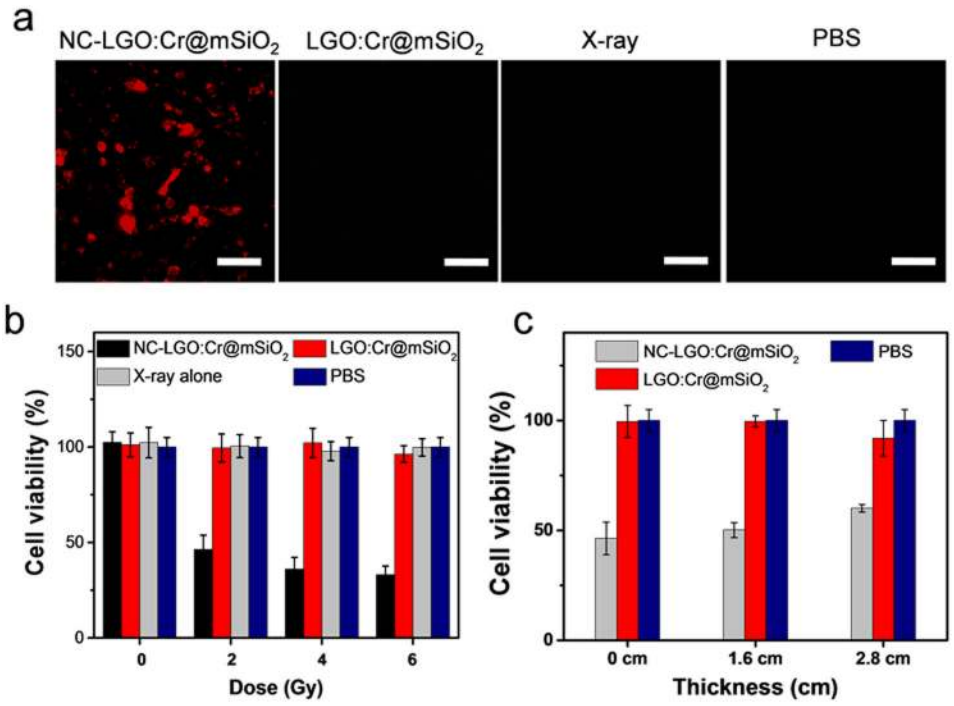

Figure 5.

In vitro viability of X-PDT. a) Ethd-1 assay for assessment of X-PDT induced cell death. In accordance with the results from Figure 4c), extensive cell death (red fluorescence, ex/em: 530 nm/635 nm) was observed when cells were treated with NC-LGO:Cr@$mSiO_2$ plus X-ray. Scale bars, 100 μm. b) Viability changes, based on MTT assays performed 24 hrs after treatments. While X-ray alone and LGO:Cr@$mSiO_2$ plus X-ray caused no viability drop, NC-LGO:Cr@$mSiO_2$ plus X-ray (i.e. X-PDT) induced efficient cell death. c) Impact of tissue depth on X-PDT efficiency. X-PDT can be stimulated from beneath thick tissues (e.g. 1.6 and 2.8 cm) to cause efficient cell death.

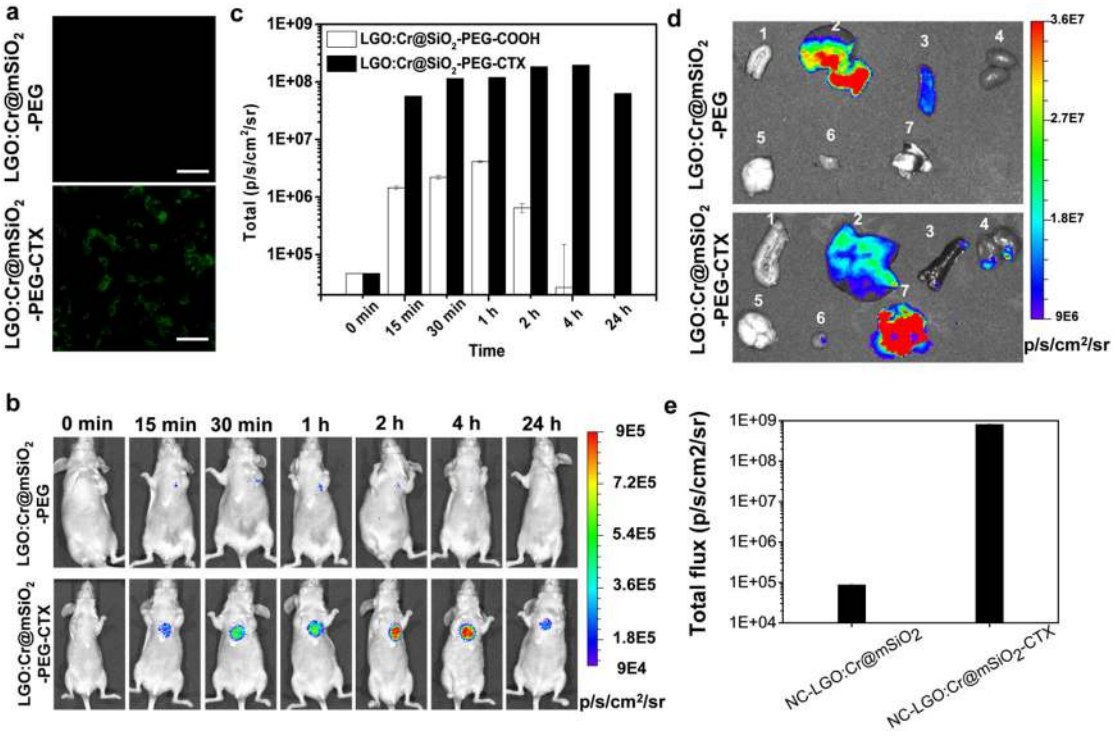

Figure 6.

Tumor targeting of NC-LGO:Cr@$mSiO_2$-CTX. a) *In vitro* microscopic analysis, conducted with H1299 cells. NC-LGO:Cr@$mSiO_2$-CTX can be efficiently internalized by H1299 cells. As a comparison, NC-LGO:Cr@$mSiO_2$ showed minimal cell uptake. Scale bars: 100 μm. b) *In vivo* imaging, based on XEOL signals and assessed in H1299 lung tumor models. NC-LGO:Cr@$mSiO_2$ and NC-LGO:Cr@$mSiO_2$-CTX nanoparticles (0.4 mg per animal) were intravenously injected to the animals. For imaging, X-ray (0.02 Gy) was applied to the lung areas, followed by immediate BLI. Strong luminescent signals in the lung were found in the NC-LGO:Cr@$mSiO_2$-CTX group but not the NC-LGO:Cr@$mSiO_2$ group. c) XEOL intensity changes, based on BLI imaging results from b). d) *Ex vivo* images with dissected tissues from b). 1. Intestine; 2. liver; 3. spleen; 4. kidneys; 5. brain; 6. muscle; 7. lung. e) Luminescent intensity changes, based on BLI imaging results from d).

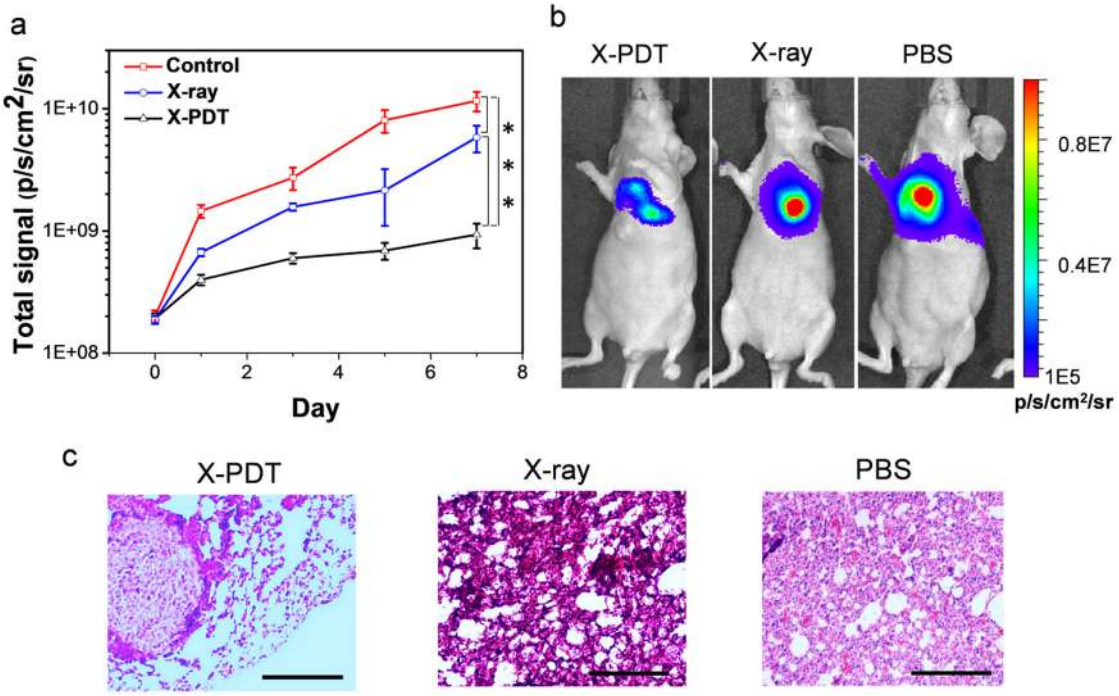

Figure 7.

In vivo therapy of X-PDT. a) Tumor growth, assessed by monitoring BLI signal changes at different time points. Compared to irradiation alone, X-PDT much more efficiently suppressed tumor growth. *** P<0.001. b) Representative BLI images for the three treatment groups, taken on Day 7. c) H&E staining on tumor tissues. Compared to the control and irradiation alone, X-PDT effectively controls the tumor generation in the lung. Scale bars, 200 μm.